INTERNATIONAL JOURNAL FOR NUMERICAL METHODS IN FLUIDS, VOL. 1, 273–290 (1981)

ASPECTS OF LARGE EDDY SIMULATION OF HOMOGENEOUS ISOTROPIC TURBULENCE

M. ANTONOPOULOS-DOMIS

Department of Nuclear Engineering, Queen Mary College, Mile End Road, London, England

SUMMARY

HOMTY, a code for Large Eddy Simulation of homogeneous isotropic turbulence is proven by successful simulation of two experiments. The role of each term in the equations of motion and the concept of filtering is examined. It is shown that 'prefiltering' is unnecessary, and the resulting additional term in the equations, instead of transferring energy to the subgrid scales, backscatters energy from the resolved large wavenumbers to the small ones. The kinetic energy decay exponent is shown to depend on the low wavenumber part of the velocity spectrum. Pressure statistics are computed and found to be in agreement with previous computations.

KEY WORDS Large Eddy Simulation Isotropic Turbulence Filtering

1. INTRODUCTION

Large Eddy Simulation (LES), the method in which the flow–geometry-dependent large scale turbulent motions are explicitly computed while the small ones—expected to be universal—are modelled, is now an established term in computational fluid dynamics. A review of the current state of the art is given in Reference 1.

The most direct and flexible simulation is by integration of the 3-dimensional time dependent Navier–Stokes equations, the differential operators of which are approximated by finite difference schemes. By its very nature the finite difference scheme (or for that matter any other technique using a digital computer) cannot resolve scales smaller than the computational grid spacing h. Whilst the raw Navier–Stokes and continuity equations describe fields which are continuous in space and time, the fields processed by the simulation are discrete. Therefore smoothed ('filtered') fields are resolved, the filtering being imposed by the discretization and the particular numerical scheme used. The effects of the unresolved scales (also known as subgrid scales (SGS)) must be modelled in terms of the resolved variables.

There have been two approaches to the definition of the resolved field. Leonard[2] defined a new field of filtered variables $\bar{f}$ by convolution of each variable f of the original field with a filter function $G(\mathbf{x})$.

$$\bar{f}(\mathbf{x}, t) = \int_{\text{all space}} G(\mathbf{x}-\mathbf{x}')f(\mathbf{x}', t)\,\mathrm{d}x' \tag{1}$$

Application of (1) yields a new set of equations, describing fields continuous in space and time. The $\bar{f}(\mathbf{x}, t)$ are regarded as the computed variables at the discrete points of the

0271-2091/81/030273-18$01.80

Received 19 November 1980
Revised 1 April 1981

computational grid. The other approach is to define the resolvable variables f at the discrete grid points (x_1, x_2, x_3) only, as averages over volumes.[3,4]

$$\bar{f} = \frac{1}{h^3} \int_{x_1-h/2}^{x_1+h/2} \int_{x_2-h/2}^{x_2+h/2} \int_{x_3-h/2}^{x_3+h/2} dx_1\, dx_2\, dx_3 f(x_1, x_2, x_3) \tag{2}$$

Let f' be the unresolved part of f. Then after an application of either of the operations (1) or (2), both of which will be denoted by an overbar, on the continuity and Navier–Stokes equations and subsequent substitution of,

$$f' = f - \bar{f} \tag{3}$$

the new equations read

$$\partial \bar{u}_i / \partial x_i = 0 \tag{4}$$

$$\frac{\partial \bar{u}_i}{\partial t} + \frac{\partial}{\partial x_j} \overline{\bar{u}_i \bar{u}_j} - \nu \frac{\partial^2}{\partial x_j^2} \bar{u}_i + \frac{\partial}{\partial x_j} R_{ij} = -\frac{\partial \bar{p}}{\partial x_i} \tag{5}$$

$$R_{ij} = \overline{u_i' u_j'} + \overline{\bar{u}_i u_j'} + \overline{u_i' \bar{u}_j} \tag{6}$$

where R_{ij} are the subgrid scale stresses which must be modelled, u_i, $i = 1, 2, 3$ are the fluctuating velocity components, p is the kinematic pressure, ν is the kinematic viscosity and the summation convention is used.

In the volume balance procedure it is evident that

$$\overline{\bar{u}_i \bar{u}_j} = \bar{u}_i \bar{u}_j \tag{7}$$

$$\overline{u_i' \bar{u}_j} = \overline{\bar{u}_i u_j'} = 0 \tag{8}$$

With the prefiltering procedure (7) and (8) are, in general, not true as Leonard[2] pointed out. For the top-hat and the Gaussian filters (see next section) he has shown that,

$$\overline{\bar{u}_i \bar{u}_j} = \bar{u}_i \bar{u}_j + \frac{\Delta_A^2}{24} \nabla^2 (\bar{u}_i \bar{u}_j) + O(\Delta_A^4) \tag{9}$$

where Δ_A is the filter width and the second term in (9) is known as the Leonard term. With this approach the Comte-Bellot and Corrsin experiment[5] on near isotropic turbulence was simulated successfully by Kwak *et al.*[6] who used a centred grid. A filter width $\Delta_A > h$ was found to be necessary, the optimum being about $\Delta_A = 2h$.

The main objective of the present work is to examine the concept of filtering. In our LES code (HOMTY) the Leonard term is included and the final equations read.

$$\partial \bar{u}_i / \partial x_i = 0 \tag{10}$$

$$\frac{\partial \bar{u}_i}{\partial t} = -\frac{\partial}{\partial x_j} (\bar{u}_i \bar{u}_j + F_L \frac{\Delta_A^2}{24} \nabla^2 \bar{u}_i \bar{u}_j - 2\nu_u S_{ij}) + \\ + F\nu \nabla^2 \bar{u}_i - \frac{\partial \bar{p}}{\partial x_i} \tag{11}$$

$$S_{ij} = \frac{1}{2} \left(\frac{\partial \bar{u}_i}{\partial x_j} + \frac{\partial \bar{u}_j}{\partial x_i} \right) \tag{12}$$

$$\nu_u = (C\Delta_A)^2 (2 S_{ij} S_{ij})^{1/2} \tag{13}$$

F_L, F are flags switching the relevant terms to 'on' or 'off'. It will be seen that the subgrid

scale stresses R_{ij}, responsible for the energy transfer to the subgrid scales, are represented by an eddy viscosity model and the Smagorinsky[7] model is used for the eddy viscosity.

For the case of homogeneous isotropic turbulence treated by HOMTY, periodic boundary conditions are assumed at the surfaces of the computational cubic box with side $L = Nh$. Details of the finite difference schemes are given by Antonopoulos-Domis and Love.[8] Here we briefly record that a staggered grid is used and that two versions of HOMTY have been tested. In the first the terms $d(\bar{u}_i\bar{u}_j)/dx_j$ and $d\bar{p}/dx_i$ are approximated to the 4th order and all other terms to the 2nd. In the second version all terms are approximated to the 2nd order. Both versions gave practically the same results.

The near isotropic velocity fields of the Comte-Bellot and Corrsin[5] and of the Yeh and Van-Atta[9] experiments are used as test-beds for the simulation. From now on the former is abbreviated to CBC and the latter to YVA. In the YVA experiment the turbulence-producing grid was heated, but the temperature fluctuations were kept sufficiently small for buoyancy forces to be negligible.

The kinetic energy decay reaches an asymptotic state in the simulation and this is compared with the 'final period of decay'.[10] The dependence of the kinetic energy decay rate on initial spectra is examined. The contribution of each term in (11) to the evolution of the velocity field is investigated and finally statistics of the pressure fluctuations are computed.

2. FILTERED VARIABLES

Whichever procedure is used the simulated fields are approximations, and should be compared, to smoothed ('filtered') versions of the experimental fields. To distinguish between the volume and the filtering procedures we use the terms 'filtered' for variables derived with the former and 'prefiltered' for variables derived with the latter. Accordingly Leonard's formalism is referred to as 'prefiltering'. On the merits of the different filters considered in prefiltering see Reference 6. The most commonly used are the Gaussian,

$$G(\mathbf{x}) = \exp\{-6\mathbf{x}^2/\Delta_A^2\} \tag{14}$$

and the top-hat filter

$$G(\mathbf{x}) = \begin{cases} 1/\Delta_A^2 & \text{at } |x_i| < \Delta_A/2 \\ 0 & \text{otherwise} \end{cases} \tag{15}$$

Their 3-dimensional Fourier transforms are

$$\text{Gaussian} \qquad G(k) = \exp\{-k^2\Delta_A^2/24\} \tag{16}$$

$$\text{top-hat} \qquad G(k) = B(k_1\Delta_A)B(k_2\Delta_4)B(k_3\Delta_A) \tag{17}$$

$$B(y) = \sin(y/2)/(y/2) \tag{18}$$

It can be readily seen that the filter inherent in the volume balance procedure is the top-hat with $\Delta_A = h$ = mesh spacing. The Gaussian filter is isotropic, whilst the top-hat is not. Quarini[11] computed the isotropic component $G_0(k)$ and the anisotropic higher harmonics of the top-hat (Figure 1) showing that the anisotropy is weak. In Figure 1 the Gaussian $G(k)$ with $\Delta_A = h$ is plotted for comparison with the top-hat. It is clear that, up to the maximum wavenumber $k_{max} = \pi\sqrt{3}/h$ that can be resolved by the simulation, their difference is for all practical purposes conceptual rather than real.

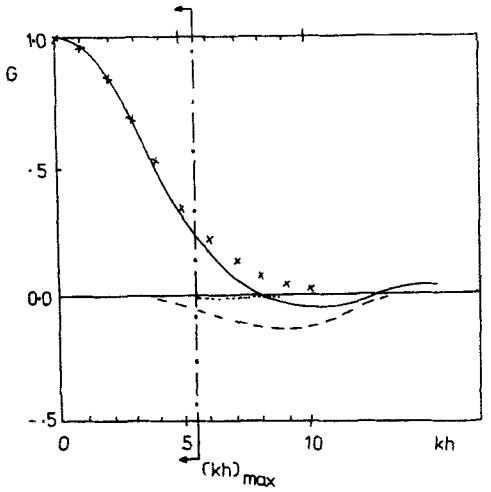

Figure 1. Comparison of filters. —— isotropic component G_0 of top-hat, - - - - - harmonic G_4^0 of top-hat, × × × × × Gaussian

The 3-dimensional filtered energy spectra $\bar{E}(k)$, to be compared with those of the simulation are obtained from the raw experimental ones $E_{exp}(k)$ as,

$$\bar{E}(k) = E_{exp}(k)\,|G(k)|^2 \tag{19}$$

and the filtered kinetic energy as,

$$0{\cdot}5\langle \bar{u}_i^2 \rangle = \int_0^\infty \bar{E}(k)\,dk \tag{20}$$

where $\langle\ \rangle$ denotes an average over the whole computational box. The longitudinal integral scale $\bar{L}$ and Taylor microscale $\bar{\lambda}$ are computed as,

$$\bar{L} = \frac{3\pi}{4} \frac{\int_0^\infty k^{-1}\bar{E}(k)\,dk}{\int_0^\infty \bar{E}(k)\,dk} \tag{21}$$

$$\bar{\lambda} = \frac{\langle \bar{u}_1^2 \rangle}{\langle (\partial \bar{u}_1/\partial x_1)^2 \rangle} \tag{22}$$

3. RESULTS

3.1. *Volume balance procedure—simulation of experiments*

The Leonard term was first switched 'off' ($F_L = 0$). The molecular viscosity term was also switched 'off' ($F = 0$) which is equivalent to lumping the difference into the subgrid term (eddy viscosity). The effect of so doing is discussed in section 3.2.

Table I. Characteristic parameters of the laboratory experiments

	Comte-Bellot and Corrsin experiment	Yeh and Van-Atta experiment
Free stream velocity U_0 (m/sec)	10·0	4·0
Grid spacing M (mm)	50·8	40·0
$R_M = U_0 M/\nu$	$3{\cdot}3\,10^4$	$1{\cdot}10^4$
$R_\lambda = u_1\lambda/\nu$	71·6	35·2
Kolmogorov microscale $\eta = (\nu^3/\varepsilon)^{1/4}$ (mm)	0·29	0·53

The initial velocity field, which must obey the continuity condition, is derived in HOMTY from a random Gaussian field; any prescribed 3-dimensional spectrum can be imposed. For the simulation of the CBC experiment the filtered experimental spectrum (cf. (19) with $\Delta_A = h$) at station $x_0/M = 42$ was imposed; M is the mesh spacing of the turbulence-producing grid and x the distance downstream from the grid. For the simulation of the YVA experiment the 3-dimensional spectrum at $x_0/M = 25$ was imposed. The characteristic parameters of these experiments are given in Table I.

Considering a co-ordinate frame convected with the mean stream velocity U_0, laboratory measurements at a distance $x - x_0$ downstream from the station x_0 correspond to our simulation results at time $t_n = n\Delta t = (x - x_0)/U_0$; n is the number of time steps and Δt the time step of the computation. For comparision with the laboratory results we present our results at stations x/M rather than the computation time t_n.

A small mesh size h is desirable, to include in the simulation as much as possible of the high wavenumber part of the spectrum ($k_{max} = \pi\sqrt{3}/h$). On the other hand $L = Nh$, N being the number of grid points in any one direction, must be large enough to include the important part of the large scales ($k_{min} = 2\pi/L$). In this simulation h was put equal to 15 mm for the 16^3 runs and to 10 mm for the 32^3 runs.

The model parameter C (equation (13)) is known to depend on a subgrid scale Reynolds number R_{SGS} and at low R_{SGS} it can be determined without recourse to experiment.[1,12] Alternatively it can be determined by tuning C to match the simulated kinetic energy decay with that of a particular experiment.[6] The latter procedure was used here and the value of C, so obtained, was found the same for both, the CBC and YVA, experiments namely

$$C = 0{\cdot}23 \tag{23}$$

In Figure 2 the simulated and experimental decay of $\langle \bar{u}_i^2 \rangle$ are compared for the 16^3 runs; C was found to be independent of the size of the mesh spacing. The 3-dimensional velocity spectra are presented in Figures 3 and 4 for the CBC experiment and in Figures 5 and 6 for the YVA experiment. It can be seen that the agreement of the simulated with the filtered experimental spectra is excellent; it is particularly encouraging the fact that HOMTY predicts the spectra at the relatively long time required to reach the station $x/M = 171$ of the CBC experiment.

Lilly[3] assuming that the mesh spacing h lies within the inertial subrange, calculated the rate $\langle T \rangle$ at which the Smogorinsky model transfers energy to the subgrid scales. Equating $\langle T \rangle$ to the dissipation rate $\langle \varepsilon \rangle$ he obtained theoretical predictions of C. Considering continuous space configuration he obtained the value $C = 0{\cdot}18$. On the other hand, approximating the

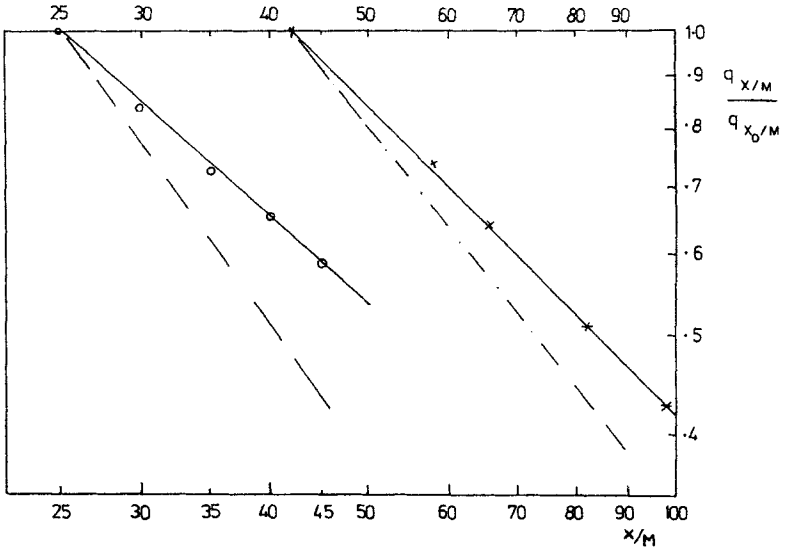

Figure 2. Decay of $q = 0{\cdot}5\langle u_i^2 \rangle$, ($C = 0{\cdot}23$, $h = 15$ mm), × × × × simulation of the CBC experiment, OOO simulation of the YVA experiment, —— filtered experimental, — — raw experimental

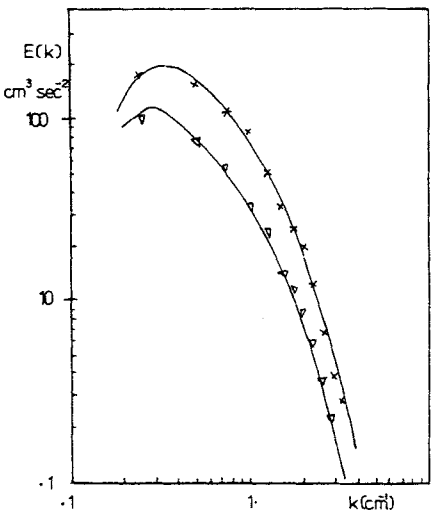

Figure 3. Three-dimensional spectra of the CBC experiment, 16^3 ($h = 15$ mm) run, × × × × simulation at $x/M = 98$, ▽▽▽▽ simulation at $x/M = 171$, —— filtered experimental

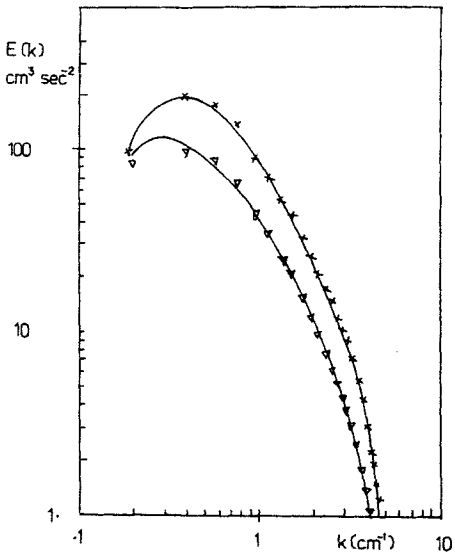

Figure 4. Three-dimensional spectra of the CBC experiment, 32^3 ($h = 10$ mm) run, × × × × simulation at $x/M = 98$, ∇∇∇ simulation at $x/M = 171$, —— filtered experimental

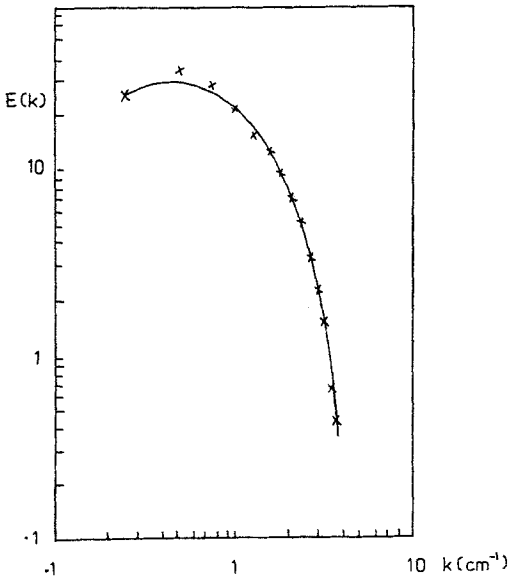

Figure 5. Three-dimensional velocity spectrum of the YVA experiment, 16^3 ($h = 15$ mm) run, × × × × × simulation at $x/M = 46{\cdot}6$, —— filtered experimental

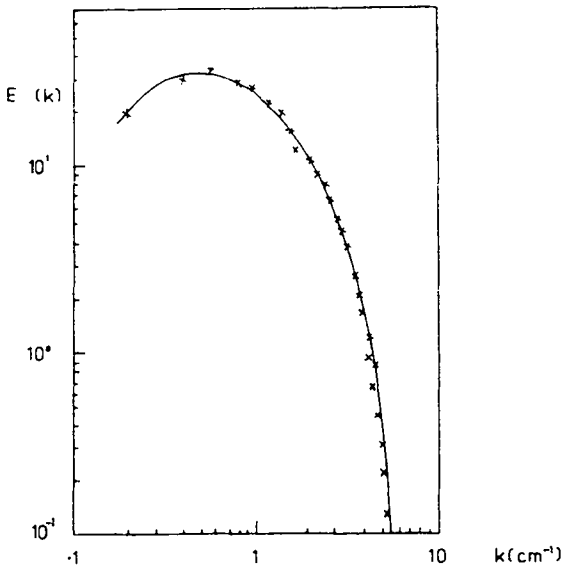

Figure 6. Three-dimensional velocity spectra of the YVA experiment at $x/m = 46{\cdot}6$, 32^3 ($h = 10$ mm) run, × × × simulation, —— filtered experimental

equations by finite difference formulae (discrete space) and replacing first derivatives by,

$$\frac{df}{dx} \triangleq \frac{\delta f}{\delta x} = \frac{1}{h}[f(x+\tfrac{1}{2}) - f(x-\tfrac{1}{2})] \tag{24}$$

he obtained the value $C = 0{\cdot}23$. The difference is significant because it arises solely by moving from the continuous to discrete space. Lilly defines his resolved variables by (2) and used (7) and (8) consistently, i.e. the volume balance procedure. First derivatives in the staggered grid of HOMTY are indeed of the form (24) and so far we have used the volume balance procedure. Thus the remarkable verification of Lilly's prediction cannot be fortuitus. In his derivation he makes the assumption,

$$\langle \bar{S}^{3/2} \rangle = \langle \bar{S} \rangle^{3/2} \tag{25}$$

$$\bar{S} = \tfrac{1}{2} S_{ij} S_{ij} \tag{36}$$

Our numerical simulations (both 16^3 and 32^3 runs) justify this assumption giving,

$$\langle \bar{S}^{3/2} \rangle / \langle \bar{S} \rangle^{3/2} \cong 1{\cdot}1 \tag{27}$$

The kinetic energy in experiments of near isotropic grid generated turbulence is found to decay as,

$$\langle u_i^2 \rangle \sim (x/M)^{-n} \tag{28}$$

where x is the distance downstream from the turbulence-producing grid with mesh spacing M. In a co-ordinate frame convected with the mean stream velocity U_0 this is equivalent to,

$$u_i^2 \sim t^{-n} \tag{29}$$

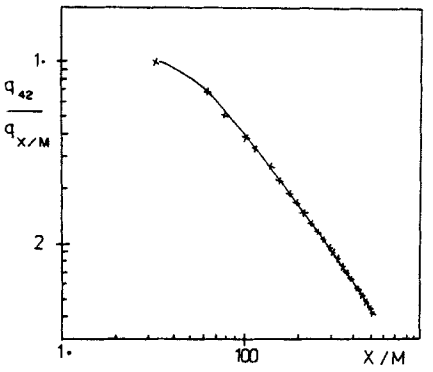

Figure 7. Decay of $q = 0{\cdot}5\langle \bar{u}_i^2 \rangle$ to asymptotic state with $n = 1{\cdot}63$

In all experiments $n = 1{\cdot}2 \pm 0{\cdot}25$ during the initial period of decay. Batchelor and Townsend[10] considered the last stages of decay during which intertia forces are negligible compared with viscous forces; they called this 'the final period of decay of turbulence'. Neglecting inertial forces they predicted an asymptotic decay law with $n = 2{\cdot}5$ during the final period and verified their deduction experimentally; the final period was reached at $x \mid M > 400$.

Using the CBC spectrum at $x/M = 42$ as the initial one, we advanced the fields of our simulation (16^3 run including molecular viscosity term) up to 250 time steps with $t =$ 0·01 sec/step which is equivalent to $x/M = 542$ in the CBC experiment. It can be seen in Figure 7 that the simulation reaches an asymptotic state with $n = 1{\cdot}63$ at x/m 300. This exponent is smaller than the $n = 2{\cdot}5$ of the 'final period'. First we should note that the exponent in the energy decay of the resolved field is always smaller than that of the raw field (Figure 2). Furthermore the dissipation by molecular viscosity within the resolved scales is a small fraction of the total; for the present runs with $h = 15$ mm this fraction is only 5 per cent, as is shown in the next section. The rest is provided for by the model (eddy viscosity) as energy transfer to the unresolved scales. Therefore the fundamental condition for the 'final period' that inertial forces are much less than viscous ones, has no chance of validity with the coarse meshes to which we are limited except at very low Reynolds numbers with Kolmogorov scales of the order of h. Of course, by varying (artificially) the ratio of eddy viscosity drain to molecular viscosity dissipation, any decay behaviour up to $n = 2{\cdot}5$ can be obtained. We may conclude that in the simulation we may talk about an asymptotic state but not of a proper 'final period' as defined by Batchelor and Townsend.[10]

Quite apart from this asymptotic state, the decay rate depends, in general, on the form of the initial spectrum and in particular on its low wavenumber part. Considering a strongly turbulent motion where viscous forces are negligible we may write (with the Smagorinsky approximation for eddy viscosity)

$$\frac{\partial E(k,t)}{\partial t} = -2\nu_u k^2 E(k,t) \tag{30}$$

$$\nu_u = F_1 \varepsilon^{1/3} h^{4/3} \tag{31}$$

$$\varepsilon = F_2 t^{-3\beta} \tag{32}$$

where F_1, F_2 are constants and β a 'constant' to be determined. From these it can be readily shown that

$$E(k, t) = E(k, 0) \exp\{-F_3 k^2 t^{1-\beta}\} \tag{33}$$

F_3 is again a constant and the dependence of the kinetic energy q,

$$q(t) = \int_0^\infty E(k, t)\, dk \tag{34}$$

on the initial spectrum $E(k, 0)$ shape is apparent. Assume for example that,

$$E(k, t) = bk^m \exp\{-F_3 k^2 t^{1-\beta}\} \tag{35}$$

Since $-dq/dt$ must be equal to ε in (32), straightforward algebra gives

$$q \sim t^{-2(m+1/m+7)} \tag{36}$$

This shows that the smaller m, i.e. the more energy there is in the largest scales the slower the decay is and this is what one would have expected, since it is the largest scales which decay slowest. Although (36) is derived on the basis of an unrealistic initial spectrum $E(k, 0) = bk^m$, it shows clearly the dependence of the decay exponent on the low wavenumber part of the intial spectrum. Schumann and Patterson[15] observed the dependence of n on initial spectra in their numerical experiments using shapes differing at both low and high wavenumbers, namely.

$$E(k, 0) = A_1 k^4 \exp\{-2(k/k_{peak})^2\} \tag{37}$$

$$E(k, 0) = A_2 k \exp\{-k/k_{peak}\} \tag{38}$$

To investigate the dependence of n on small k's we used four initial spectra (Figure 8), all of them having at large k's the shape of the CBC spectrum at $x/M = 42$; the initial energy was for all of them that of the CBC at $x/M = 42$. The resulting exponents n are plotted in Figure 9 versus the initial Taylor microscales; the numbering agrees with that of Figure 8. A trend of increasing n with decreasing scales can be observed and since the initial energy was the same for all of these runs, this figure can be read as n versus $R_\lambda = u\lambda/\nu$. As expected, with the peak of the spectrum moving towards larger k's the energy decays faster.

In the YVA experiment the evolution of the integral scales is presented. Clearly the scales of the resolved field are larger than the raw ones and the larger the mesh spacing h, the larger the computed scales would be. The integral scales of the simulation are compared to the filtered experimental ones in Figure 10(a); the agreement is excellent as would be expected from the good agreement on spectra. In the same figure the evolution of computed Taylor microscales of the YVA experiment is presented and Figure 10(b) gives the scales of the CBC experiment as obtained from the simulation.

From the result discussed so far we may conclude that:

(a) the volume balance procedure is capable of predicting the evolution of the velocity field statistics. The good agreement between simulation and laboratory experiments shows that inclusion of the Leonard term, hence application of prefiltering, is not necessary for such an agreement. Recalling that inclusion of this term required a filter width larger than h, the success of the volume balance procedure shows that scales down to the mesh spacing h, as opposed to the filter width with prefiltering, can be resolved.

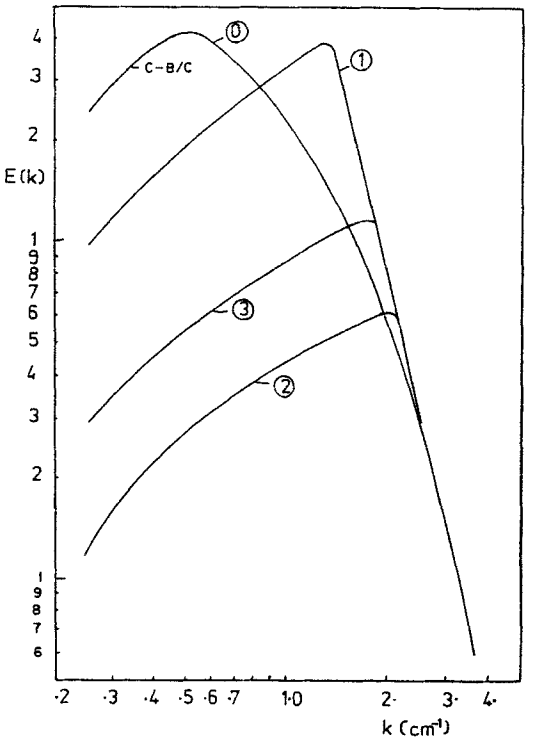

Figure 8. Shapes of initial velocity spectrum, 16^3 runs. Vertical scale arbitrary

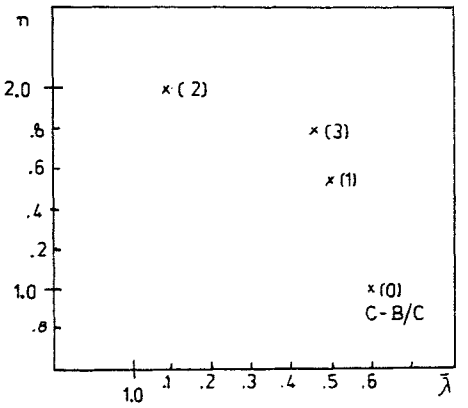

Figure 9. Dependence of decay exponent n on initial spectra (Figure 8). $\bar{\lambda}$ is the initial velocity Taylor microscale. 16^3 runs

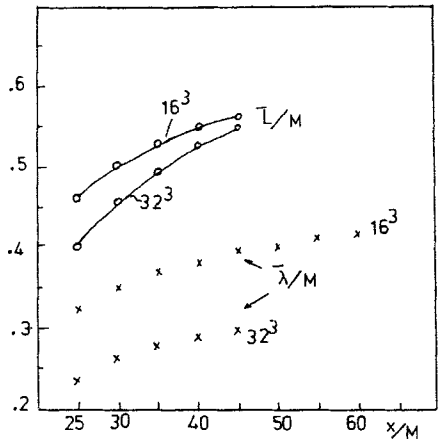

Figure 10(a). Velocity scales of the YVA experiment. 16^3 and 32^3 runs, —— —— filtered experimental integral scales, O and × simulation

(b) the effects of the subgrid scales are successfully modelled by the Smogorinsky model in isotropic flows. The model parameter was found in agreement with Lilly's prediction and independent of the mesh size h.

3.2. *Prefiltering—role of each term in the equations*

For the range of scales in the CBC and YVA experiment a mesh size of $h = 15$ mm in 16^3 grid-box runs is sufficient to simulate the field evolution, as shown in Section 3.1. Therefore investigation of the role of each term in the equations was done with 16^3 runs and the initial field statistics of the CBC experiment at $x/M = 42$.

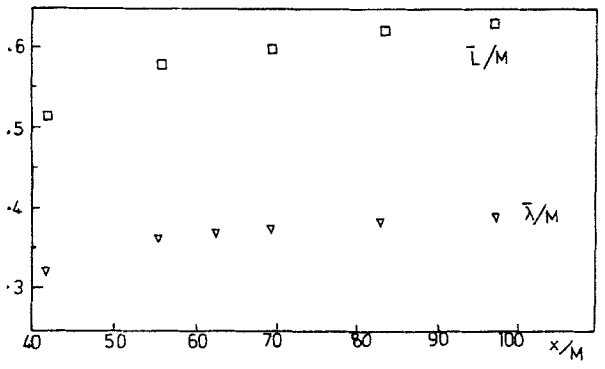

Figure 10(b). Velocity scales from the simulation of the CBC experiment, 16^3 runs

First the molecular viscosity and Leonard terms were switched 'off' and the model parameter was set equal to 0. The computation is then following the evolution of a field u_i which obeys (10) and

$$\frac{\partial \bar{u}_i}{\partial t} + \frac{\partial \bar{u}_i \bar{u}_j}{\partial x_j} = -\frac{\partial \bar{p}}{\partial x_i} \tag{39}$$

The finite difference approximation to $\partial \bar{u}_i \bar{u}_j / \partial x_j$ is energy-conserving and therefore the energy was constant for all time steps. The spectral results are shown in Figure 11 where it can be seen that the convective term transfers energy, as it should, from small wavenumbers k to large ones, with a sharp cut-off at the maximum resolvable k. Bearing in mind that the only term additional to (39) in the equations of the previous section is the subgrid term, it is clear that the latter transfers energy from the high wavenumber part of the resolved scales to the subgrid scales, which is exactly what is meant to do.

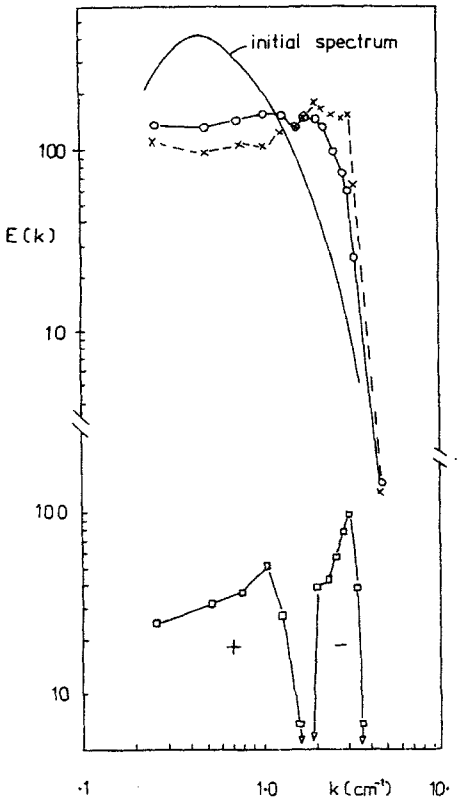

Figure 11. Effects of convective and Leonard terms. Results at 28th time step, (16^3 runs), × × × field of equation (39), ○○○ field of equation (40), □□□ Leonard term effect (subtracting × from ○)

The calculation was then repeated with exactly the same initial conditions and the Leonard term included with $\Delta_h = h$ and $C = 0$. The computation then follows the evolution of a field which obeys (10) and,

$$\frac{\partial \bar{u}_i}{\partial t} + \frac{\partial}{\partial x_j}\left(\bar{u}_i\bar{u}_j + \frac{h^2}{24}\nabla^2\bar{u}_i\bar{u}_j\right) = -\frac{\partial \bar{p}}{\partial x_j} \tag{40}$$

The principal element in Leonard's reasoning is that prefiltering should and would provide a substantial (more than 30 per cent) part of the energy transfer to the subgrid scales. In our runs the kinetic energy of the field obeying (40) remained practically constant with time. The contribution of the Leonard term to the drain of energy was also found negligible in the simulation of Kwak *et al.*[6] where a centred grid was used. Therefore its failure to provide significant energy drain cannot be attributed to the form of the computational grid. Indeed Leonard's arguments do not in any way rely on that. Our spectral results are presented in Figure 11. Subtracting the spectral values of the field satisfying (40) from those of the field which obeys (39) (both at the 28th time step) we get the effect of the Leonard term. It can be seen (Figure 11) that instead of this term draining energy to the SGS it backscatters energy from the large resolved wavenumbers to the small ones. Recalling that energy-conserving 4th and 2nd-order approximations were used for $\partial\bar{u}_i\bar{u}_j/\partial x_j$, this behaviour cannot be attributed to the numerical scheme used to approximate the convective term either. We tentatively suggest that the discrepancy between the theory of prefiltering and the results of the numerical experiments may well lie in the fact that the prefiltering approach is attempting to predict the evolution of a continuous field, whilst the simulation is processing discrete configurations.

Finally the effect of the molecular viscosity was investigated. All terms in (11) were included apart from the Leonard term. The value of C matching the experimental decay was now found to be 0·22 rather than 0·23. The rate of dissipation $\varepsilon_{\nu,\mathrm{res}}$ by molecular viscosity within the resolved scales depends on the ratio η/h, where η is the Kolmogorov microscale. To estimate $\varepsilon_{\nu,\mathrm{res}}$ we have used the dissipation spectrum proposed by Pao[13]

$$D(k) = 2\nu K_0 \varepsilon^{2/3} k^{1/3} \exp\{-1{\cdot}5K_0(k\eta)^{4/3}\} \tag{41}$$

where $K_0 \simeq 1{\cdot}5$ is Kolmogorov's constant. This gives the fraction of the energy rate ε_k dissipated by viscosity below wavenumber k as

$$\frac{\varepsilon_k}{\varepsilon} = 1 - \exp\{-1{\cdot}5K_0(k\eta)^{4/3}\} \tag{42}$$

Leslie and Quarini[14] show that a finite difference scheme on a mesh of width h is equivalent to a sharp cut at a wavenumber $2{\cdot}957/h$. Thus Pao's spectrum gives,

$$\varepsilon_{\nu,\mathrm{res}}/\varepsilon = 1 - \exp\{-9{\cdot}5(\eta/h)^{4/3}\} \tag{43}$$

which for $h = 15$ mm and the CBC experiment ($\eta = 0{\cdot}3$) gives

$$\varepsilon_{\nu,\mathrm{res}}/\varepsilon \cong 4{\cdot}9 \text{ per cent} \tag{44}$$

Comparing the energy decay of the runs which include molecular viscosity to those which do not, we obtained the fraction of $\bar{\varepsilon}_{\nu,\mathrm{res}}$ to the total rate of decay $\bar{\varepsilon}_{\mathrm{total}} = \mathrm{d}q/\mathrm{d}t$

$$\bar{\varepsilon}_{\nu,\mathrm{res}}/\varepsilon_{\mathrm{total}} \simeq 4{\cdot}8 \text{ per cent} \tag{45}$$

in agreement with (44). The fact that 5 per cent of $\varepsilon_{\mathrm{total}}$ is dissipated by molecular viscosity is consistent with the 5 per cent reduction of C, when molecular viscosity was included.

3.3. *Pressure fluctuations*

Schumann and Patterson[15] integrated a discretized version of the Navier–Stokes equations without any SGS modelling at low Reynolds numbers using the spectral method of Orszag[16] to study pressure and velocity fluctuations in isotropic turbulence. Their initial velocity spectral shapes are those of (37) and (38). They quote 'experimental' values of the ratio $\langle p^2\rangle^{1/2}/\langle u_1^2\rangle$, where the pressure fluctuations were derived from 2nd-order velocity correlations and the assumption of Gaussian velocity distribution. The 'laboratory' values, so derived, are about 0·7 which gives

$$\langle p^2\rangle^{1/2}/0{\cdot}5\langle u_i^2\rangle \simeq 0{\cdot}47 \tag{46}$$

Their computations gave $\langle \bar{p}^2\rangle^{1/2}/\langle \bar{u}_1^2\rangle$ fluctuating with time around values ranging from 0·8 to 1, i.e.

$$\langle \bar{p}^2\rangle^{1/2}/0{\cdot}5\langle \bar{u}_i^2\rangle \simeq 0{\cdot}53 \text{ to } 0{\cdot}66 \tag{47}$$

From their four runs they found the dependence of this ratio on the initial velocity spectrum to be small.

The evolution of the 3-dimensional pressure spectra obtained from our simulation of the CBC experiment is presented in Figure 12. The variation with time of the normalized rms pressure is presented in Figure 13 where it can be seen that it is fluctuating with time around a mean of

$$\langle \bar{p}^2\rangle^{1/2}/0{\cdot}5\langle \bar{u}_i^2\rangle \simeq 0{\cdot}53 \tag{48}$$

which is close to the 'laboratory' values and to those obtained by Schumann and Patterson. Similar results were obtained from the simulation of the YVA experiment.

The dependence of the normalized rms pressure on initial velocity spectra and length scales was obtained from the results of the CBC and YVA simulation and the runs with the initial spectra of Figure 8. In Figure 14 this is plotted versus the initial Taylor microscales $\bar{\lambda}$ of velocity. The numbering corresponds to that in Figure 8. It can be seen that the dependence of the rms pressure on initial velocity spectra is small, but there seems to be a trend for $\langle p^2\rangle^{1/2}/\langle u_i^2\rangle$ to increase with increasing scales.

4. CONCLUSIONS

Two LES procedures were investigated. The volume balance procedure, applied on the staggered grid of HOMTY, was capable of predicting the evolution of the statistics of homogeneous isotropic turbulence experiments. It has been shown that the Leonard term is not necessary and the same is therefore true for prefiltering. This term instead of transferring kinetic energy to the subgrid scales, backscatters energy from the resolved large wavenumbers to the small ones.

An asymptotic decay with exponent $n = 1{\cdot}63$ was reached by the simulation, but the proper 'final period of decay' with $n = 2{\cdot}5$ cannot be reproduced with the coarse meshes to which we are at present limited, except at very low Reynolds numbers. The decay exponent n is shown to depend on the low wavenumber part of the initial velocity spectrum and a trend of increasing m with decreasing velocity Taylor microscales was observed.

Pressure spectra were computed and the rms pressure normalized with kinetic energy was found to agree with previous computations. A trend for the normalized rms pressure to

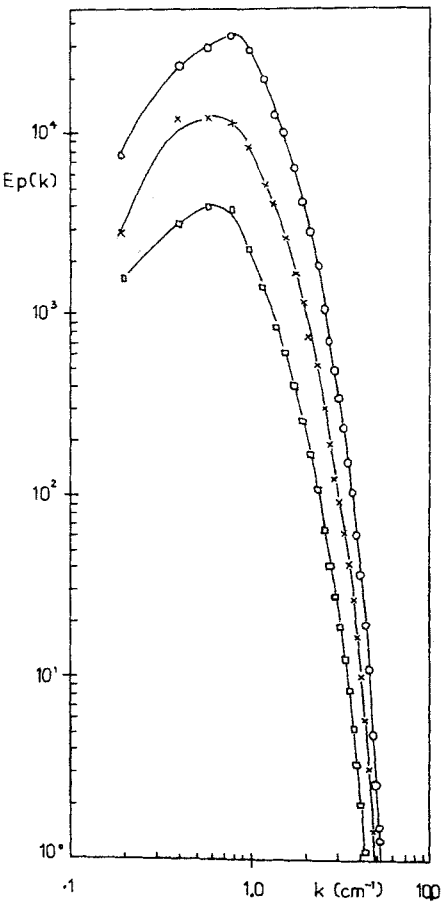

Figure 12. Three-dimensional pressure spectra. Simulation of CBC experiment, (32^3 run), ○○○ $x/M = 64$, × × × $x/M = 98$, □□□ $x/M = 171$

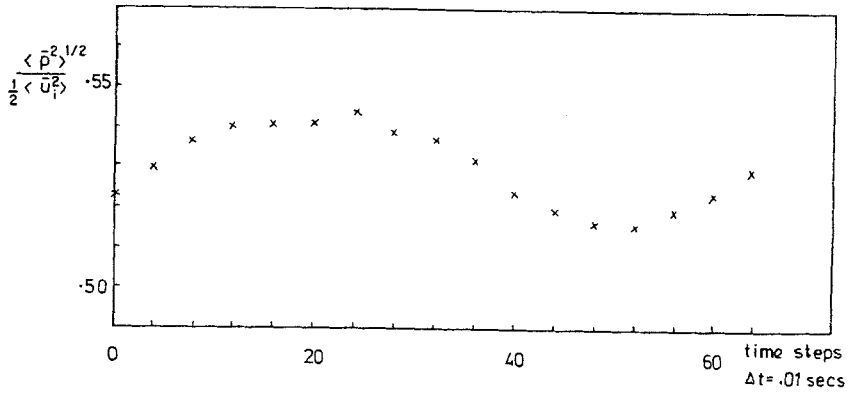

Figure 13. RMS pressure variation with time. Simulation of the CBC experiment, 16^3 run

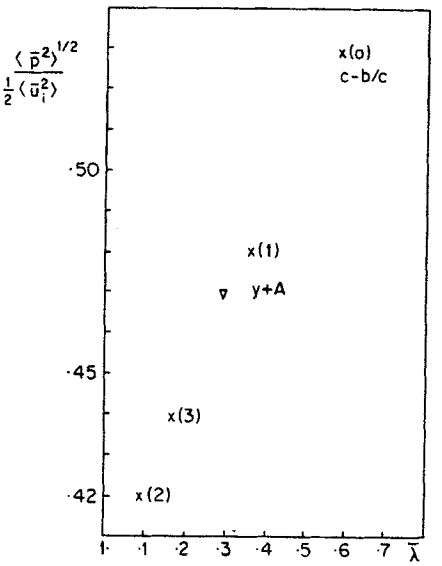

Figure 14. Normalized RMS pressure for different initial velocity spectra (see Figure 8). $\bar{\lambda}$ is the initial velocity Taylor microscale

increase with increasing velocity scales was observed but its dependence on initial velocity spectra was found to be weak.

ACKNOWLEDGEMENTS

The code HOMTY is an extension of the isotropic velocity field code FORTY, which was developed and tested by Dr. M. D. Love, Dr. S. T. B. Young and the present author, of the Turbulence Unit, Nuclear Engineering Department, Queen Mary College. The author is grateful to Drs Love and Young and to Professor D. C. Leslie for many helpful discussions.

Turbulence research in the Department of Nuclear Engineering at QMC is supported by the SRC.

REFERENCES

1. J. H. Ferziger and D. C. Leslie 'large eddy simulation: a predictive approach to turbulent flow computation', *AIAA paper No. 79/1471* (1979).
2. A. Leonard, 'Energy cascade in large eddy simulation of turbulent fluid flows', *Advances in Geophysics*, **18A**, 237–248 (1974).
3. D. K. Lilly, 'On the application of the eddy viscosity concept in the inertial subrange of turbulence', *NCAR report 123* (1966).
4. U. Schumann, 'Subgrid scale model for finite difference simulations of turbulent flows in plane channels and annuli', *J. Comp. Phys.*, **18**, 376–404 (1975).
5. G. Comte-Bellot and S. Corrsin, 'Simple Eulerian time correlation of full and narrow band velocity signals in grid generated turbulence', *JFM*, **48** (2), 273–337 (1971).
6. D. Kwak, W. C. Reynolds and J. H. Ferziger, 'Three dimensional time dependent computation of turbulent flow', *Stanford University Report No. TF-5* (1975).
7. J. Smagorinsky, 'General circulation experiments with primitive equations', *Mon. Wea. Rev.*, **93** (3), (1963).

8. M. Antonopoulos-Domis and M. D. Love, 'The finite difference schemes used in the LES code FORTY', *QMC EP 6032* (1979).
9. T. T. Yeh, and C. W. Van-Atta, 'Spectral transfer of scalar and velocity fields in heated grid turbulence', *JFM*, **58** (1), 233–261 (1973).
10. G. K. Batchelor and A. A. Townsend, 'Decay of turbulence in the final period', *Proc. Roy. Soc.*, **A194**, 527–543 (1948).
11. G. L. Quarini, 'Applications of closed turbulence theories at high wavenumbers', *Ph.D. Thesis*, QMC, University of London, 1977.
12. McMillan and J. H. Ferziger, 'Direct testing of subgrid scale models', *AIAA paper 79/0072* (1979).
13. Y. Pao, 'Structure of turbulent velocity and scalar fields at large wavenumbers', *Phys. Fluids*, **8**, 1063 (1965).
14. D. C. Leslie and G. L. Quarini, 'The application of turbulence theory to the formulation of subgrid modelling procedures', *JFM*, **91** (1), 65–91 (1979).
15. U. Schumann and G. S. Patterson, 'Numerical study of pressure and velocity fluctuations in nearly isotropic turbulence', *JFM*, **88** (4), 685–709 (1978).
16. S. A. Orszag, 'Numerical simulation of incompressible flow within simple boundaries. I. Garlekin (spectral) representations', *Stud. Appl. Math.*, **50**, 293–327 (1971).